$Au_{329-x}Ag_x(SR)_{84}$ Nanomolecules: Plasmonic Alloy Faradaurate-329

Chanaka Kumara,[a] Xiaobing Zuo,[b] David Cullen,[c] Amala Dass [a,*]
[a] *Department of Chemistry and Biochemistry, University of Mississippi, Oxford, Mississippi 38677,USA.*
[b] *X-ray Science Division, Advanced Photon Source, Argonne National Laboratory, Argonne, Illinois 60439, USA.*
[c] *Materials Science and Technology Division, Oak Ridge National Laboratory, Oak Ridge, Tennessee 37831, USA.*

ABSTRACT: Though significant progress has been made to improve the monodispersity of larger (> 10 nm) alloy metal nanoparticles, there still exists a significant variation in nanoparticles composition, ranging ± 1000's of atoms. Here, for the first time, we were report the synthesis of atomically precise (±0 metal atom variation) $Au_{329-x}Ag_x(SCH_2CH_2Ph)_{84}$ alloy nanomolecules. The composition was determined using high resolution electrospray ionization mass spectrometry. In contrast to larger (> 10 nm) Au-Ag nanoparticles, the surface plasmon resonance peak red shifts upon increasing silver content. The intensity of SPR peak also varies in an intriguing manner, where a dampening is observed with medium silver incorporation, and a significant sharpening is observed upon higher Ag content. The report outlines a) an unprecedented advance in nanoparticle mass spectrometry of high mass at atomic precision; and b) the unexpected optical behavior of Au-Ag alloys in the region where nascent SPR emerges.

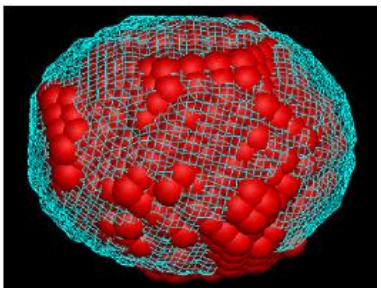

Manipulating light at the nanoscale manifested as the surface plasmon resonance (SPR) is of tremendous fundamental interest, with the potential for applications in sensing, medicine,[1] and material science.[2] Gold nanoparticles show SPR at ~530 nm, whereas SPR in silver shows at ~400 nm. Ultra-small gold nanomolecules or nanocrystal molecules[3] such as $Au_{25}(SR)_{18}$, $Au_{25-x}Ag_x(SR)_{18}$, $Au_{38}(SR)_{24}$ exhibit distinct optical features that are molecule-like, whereas $Au_{144}(SR)_{60}$ and $Au_{144-x}Ag_x(SR)_{60}$ show the relatively smooth spectra at room temperature, which lies in between molecules and plasmonic nanoparticles.[4, 5] This molecule-like to bulk transition is also reflected in the size-dependent electrochemical redox behavior.[6] Some of these materials are chiral[7] and have been used as catalysts.[8, 9] There are number of reports on the synthesis of atomically monodisperse ultra-small alloy nanomolecules[10] based on silver,[11, 12] copper,[13] palladium,[14] and platinum[15] atom incorporation. Recent progress has been made to study plasmonic nanomolecules,[16] such as $Au_{329}(SR)_{84}$, $Au_{\sim500\pm10}(SR)_{\sim120\pm3}$, and $Au_{\sim940\pm20}(SR)_{\sim160\pm4}$. $Au_{329}(SR)_{84}$ is the only nanomolecule, with ± 0 atom variation that also displays a SPR feature, making it an ideal candidate for studying the origin of plasmon resonance.[16-19] DFT based theoretical analysis[20] is currently hindered by the lack of X-ray crystal structure of plasmonic particles, though significant progress has been made in smaller crystal sizes,[21-24] and theoretical models.[25]

In general, method for the compositional analysis of larger (> 5 nm diameter) alloy nanoparticles includes energy dispersive X-ray spectroscopy (EDX), X-ray photoelectron spectroscopy (XPS), scanning transmission electron microscopy (STEM), and inductively coupled plasma mass spectrometry (ICP-MS).[26] However, these methods are limited to the determination of composition as percentage or as molar fractions with certain error limits. Electrospray ionization mass spectrometry (ESI-MS) of ultra-small nanoparticles can yield composition to the atomic level yielding specific number of metal atoms and ligands.[27-29] Recently, we have determined the atomic composition of several giant plasmonic gold nanoparticles including the 329-, ~500- and ~940-Au atom species.[12, 13, 14] However, in the cases of alloy nanomolecules, the MS based atomic level compositional determination has been limited to $Au_{25-x}Ag_x(SR)_{18}$, $Au_{38-x}Ag_x(SR)_{24}$, $Au_{144-x}Ag_x(SR)_{60}$, nanomolecules.[11, 30, 31] This is due in part to challenges in the larger (> 144-atom) species in terms of, (a) nanoparticle purification methodologies[32] to isolate pure species; and b) nanoparticle characterization methods at the atomic level to determine the composition to atomic precision. It is of great scientific interest and challenge to synthesize plasmonic alloy nanocrystals with well-defined atomic compositions to understand the emergence of SPR[33, 34] and its effect on silver alloying.[35]

Here, we report unprecedented advances in (a) the synthesis and isolation of $Au_{329-x}Ag_x(SR)_{84}$ alloy nanomolecules; (b) the atomic level composition determination by high resolution ESI-MS, counting the number of Ag atoms in a Au plasmonic nanoparticle for the first time; (c) the Au:Ag composition-electronic structure correlation, including the unusual red shift and non-linear dependence of SPR peak intensity with increasing Ag content. This unusual dependence of SPR peak necessitates the confirmation of the purity of the samples, including the exclusion of larger particles, segregated Au only and Ag only particles, and to demonstrate that all the particles are 329-metal atom based. Conclusive supporting evidence for the constant 2.2 nm diameter of all the 329-atom particles are presented in the form of small angle X-ray scattering (SAXS) measurements. The purity of the samples are shown by matrix-assisted laser desorption ionization mass spectrometry (MALDI-MS) data and high resolution ESI-MS data eliminates the possibility of segregated Au-only or Ag-

only particles. The elucidation of X-ray crystal structure and theoretical analysis will explain the intriguing optical properties of these 329-metal atom AuAg alloy nanoparticles.

Results and discussion

The synthesis of $Au_{329-x}Ag_x(SR)_{84}$ nanomolecules involves three steps, including a crude mixture preparation, followed by thermochemical treatment and solvent fractionation to purify the nanomolecules. The silver content of $Au_{329-x}Ag_x(SR)_{84}$ was changed by varying the $HAuCl_4$:$AgNO_3$ molar ratios from 1:0 to 1:1 in the initial synthesis. The composition of the Au and Ag was determined by ESI-MS to atomic precision as discussed later. The method development for this interesting atomically precise plasmonic nano-alloy synthesis origin through the combination of concept/ experience gain by Au/Ag alloy nanomolecules synthesis[31] couple with monometallic -super stable plasmonic nanoparticles synthesis protocol.[16] Several set of trials over the past few years with more experience lead to the plasmonic alloy synthesis, isolation and composition analysis as summarized in the experimental section.

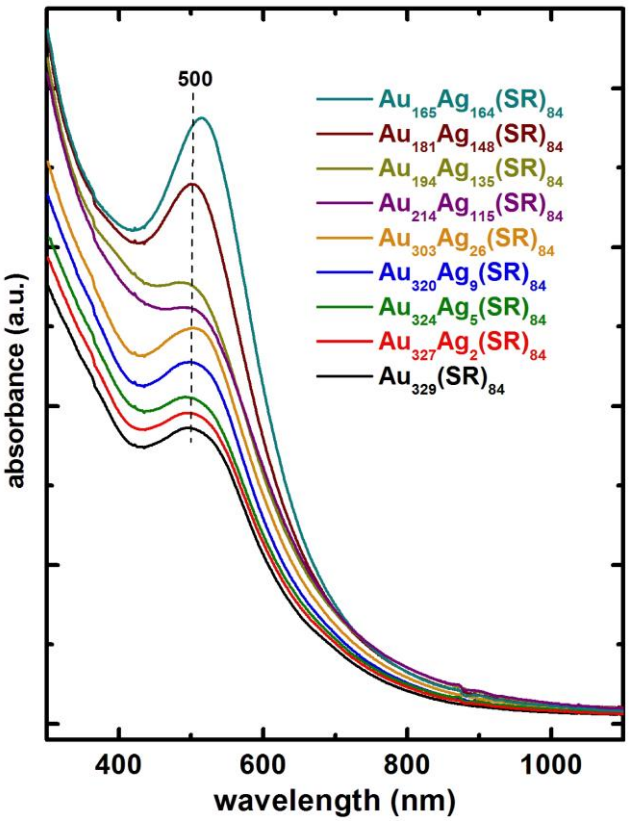

Figure 1: UV-vis spectra of $Au_{329-x}Ag_x(SR)_{84}$ nanomolecules in toluene. Au : Ag precursor ratios of 1:0 (black), 1:0.01 (red), 1:0.05 (Olive), 1:0.10 (Blue) and 1:0.20 (orange),1:0.33 (purple) and 1:0.50 (Dark yellow), 1:0.66 (Brown) and 1:1(Dark cyan) in the starting material (Spectra are offset for clarity)

Figure 1 bottom spectrum (black) shows a SPR band at 490 nm observed for Au-only $Au_{329}(SR)_{84}$ nanomolecules. No significant changes were observed in the Au:Ag ratios of 1:0 to 1:0.20. This is due to the low amount of Ag atoms incorporated in the samples. In the 0.01, 0.05, 0.1, and 0.2 ratios, an average of only 2, 5, 9 and 26 Ag atoms are incorporated into the 329-metal atom structure. The SPR band of the Au:Ag ratio at 1:0.33 and 1:0.50 containing 115 and 135 Ag atoms respectively, actually diminish compared to that of $Au_{329}(SR)_{84}$. This damping effect may due to the addition of silver in a specific geometric shell in the atomic structure which lead to the damping at Au/Ag interface or atomic structure modification upon alloying.[36] The SPR band in the mole ratio of 1:0.66 resulted in an incorporation of 148 Ag atoms on average, 45% of total metal atoms, which produces a narrow and more symmetric SPR peak ~510 nm. For intermixed or alloy Au-Ag clusters single SPR band was observed which varied between 400 to 530 nm with element composition, whereas, for core-shell nanoparticles, the SPR band red or blue shift depends on outermost shell composition and thickness.[26] Optical properties of smaller core–shell type nanoparticles also vary depending on composition, electronic structure, size, internal structure and geometry.[35] In a neutral charge state, $Au_{329}(SR)_{84}$ nanomolecules have 245 free electrons which originate from Au(6s).[20] Upon alloying the electronic states originate from both Ag(5S) and Au(6S) states.[37] Thus silver atoms enhance the degeneracy of the electron shell.[37] Sharpening of the Au plasmonic resonance was observed upon alloying which indicate the modulation of SPR by Ag. This sharpening may be due to the contribution from the imaginary part of the dielectric constant (ε_i) of the incorporated silver atoms.[36] Gold-silver nanoparticles, upon an increasing mole ratio of silver shows a SPR band that blue-shifts linearly.[38] In present study, large change in SPR peak position, ~100nm blue shift,[38] was not observed up to 1:1 Au/Ag ratio. On the contrary, a maximum of ~10nm red shift was observed and a non-linear dependence of SPR peak intensity was observed. This suggests the synthesized plasmonic nanostructure are core/shell type structure with Au rich surface or Au@Au/Ag@Au multi-shell structure.[35] The lack of X-ray structure thus far has impeded theoretical analysis to fully understand the unusual behavior of the $Au_{329-x}Ag_x(SR)_{84}$ alloy nanomolecules. The plasmonic peak of the title compounds does not have very sharp and intense peak as naked or very large gold nanoparticles which has thousand of metal atoms. However, plasmonic peak position were measured in solvents of different refractive indices (THF-1.407,$CHCl_3$-1.445 toluene-1.497) to investigate the plasmonic nature of the nanomolecules. Nanomolecules with three different Au:Ag ratio were examined. Au:Ag, 1:0 and 1:1 ratio shows significant plasmonic peak shifting to higher wavelength in high-refractive index solvent when compared to the Au:Ag 1:0.66 ratio (refer figure S11). Thus, still the electromagnetic fields of Au/Ag core feel the dielectric environment at the bulk interface, despite the ligand shell surrounding at the gold/alloy nanoparticles.

High resolution ESI-MS was used to determine the composition of the title compound, including the number of Au and Ag atoms to atomic precision. To our knowledge, this is the first report on accurate *silver atom counting* in silver alloys *of gold plasmonic nanomolecules* using mass spectrometry. ESI-MS spectra obtained for nanomolecules synthesized with 1:0.10 incoming Au-Ag molar ratios is shown in Figure 2a. ESI-MS shows multiple charged ions at 37.7, 25.2, 19 and 15 kDa corresponding to the 2-, 3-, 4- and 5- of the intact molecular ions respectively, Figure S1. The 4- charge states were predominant in the ESI spectra and the inset shows the expansion of 4- ions. The spacing between each of these peaks correspond to ~89/4 m/z, which is

the mass difference between gold, 197 Da and silver, 108 Da. Introducing silver in the form of $AgNO_3$ into the initial synthesis lead to the formation of $Au_{320}Ag_9(SR)_{84}$ alloy nanomolecules. Although nine silver atoms are incorporated into the nanomolecule, the total number of metal atoms still remains at 329. Figure S2 shows the deconvoluted ESI-MS spectra for synthetic preparations corresponding to Au:Ag precursor ratios of 1:0.10. The molecular ions were obtained by multiplying the ESI peaks corresponding to various charge states by the corresponding charge to obtain the deconvoluted 1- molecular ions. The molecular ions from 2-, 3-, 4- and 5- are in good agreement with each other adding further validity to ESI data and the observed size distribution.

The Au:Ag incoming mole ratio was gradually increased starting from 1:0 to 0.20 in the first set of experiments. In the next set of experiment, incoming mole ratio vary from 1:0.33 to 1:1. Figure 2b shows the 4- ions in the ESI-MS spectra of the alloy synthesis up to 1:0.20 incoming ratio. The bottom black spectrum shows the $Au_{329}(SR)_{84}$ plasmonic nanomolecules with no silver addition. Upon silver addition in step 1, the $Au_{329}(SR)_{84}$ mass peak shifts to the low mass region resulting in an envelope of peaks with 89/4 mass difference due to the silver incorporation. The average silver atom incorporation was 2, 5, 9 and 26 as the incoming ratio was increased to 0.01, 0.05, 0.10 and 0.20 respectively. The observation of these silver doped $Au_{329-x}Ag_x(SR)_{84}$ species further validates the reported formula 329:84. (See the supporting information table S2 and S3 for theoretical and experimental mass spectrometric values). It is interesting to note that the Au:Ag, 1:0.01 ratio shows the minor peak envelope to the right of the title compound, corresponding to $Au_{330-x}Ag_x(SCH_2CH_2Ph)_{86}$ and $Au_{331-x}Ag_x(SCH_2CH_2Ph)_{88}$ assignment.

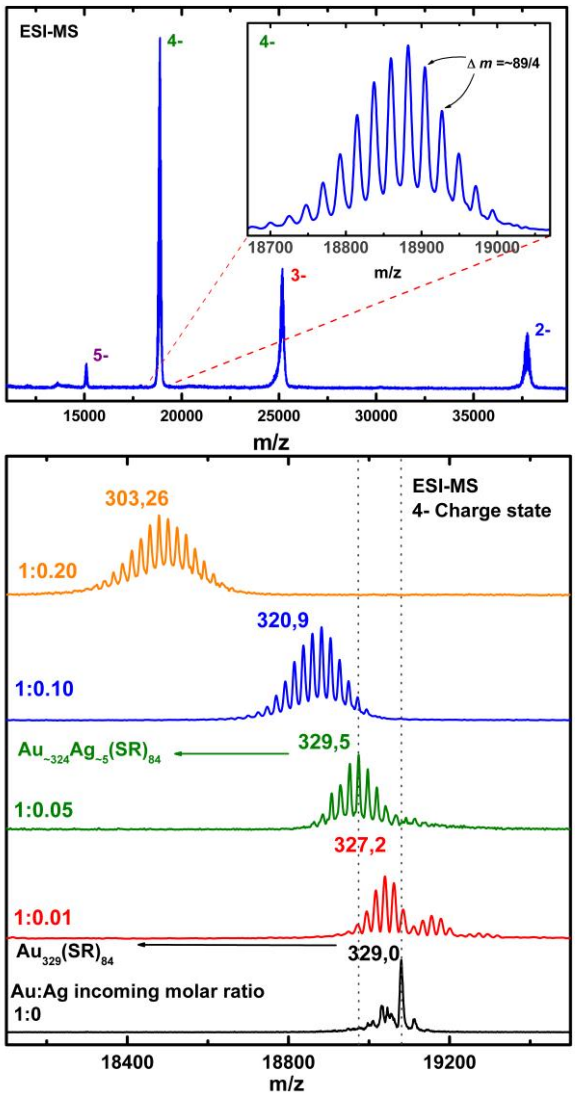

Figure 2. (Top) Electrospray ionization (ESI) mass spectrum of $Au_{329-x}Ag_x(SR)_{84}$ nanomolecules for Au:Ag precursor ratios of 1:0.10. Inset show expansion of the 4- molecular ion. The mass difference between the peaks in nanoalloys corresponds to the Au (196.97 Da) and Ag (107.87 Da) mass difference, Δ*m*=89 Da. (Bottom) ESI of $Au_{329-x}Ag_x(SR)_{84}$ nanomolecules for different Au:Ag precursor ratios. ESI mass spectrum of $Au_{329-x}Ag_x(SR)_{84}$ nanomolecules for incoming Au:Ag precursor ratios of 1:0 (black), 1:0.01 (red), 1:0.05 (olive), 1:0.10 (blue) and 1:0.20 (orange).

For smaller gold and alloy nanoparticles like $Au_{25}(SR)_{18}$ and $Au_{25-x}Ag_x(SR)_{18}$, there exists only one major species. However for larger alloy nanoparticles, such as $Au_{144-x}Ag_x(SR)_{60}$, there are other closely related $Au_{144-x}Ag_x(SR)_{59}$ species,[31] while the 144:60 is the dominant species.

Figure 3(left) shows the MALDI spectra taken for the $Au_{329-x}Ag_x(SR)_{84}$ synthesized using different incoming molar ratio. The good baseline indicates the purity of the nanoparticles, including the absence of 144-Au atom species and larger plasmonic particles. Until the Au:Ag incoming molar ratio reach 1:0.20, no significant mass shift was observed upon silver atom incorporation. However, nanomolecules synthesized using 1:0.20 to 1:1 show

clear mass shifting to the low mass region in MALDI spectra compared to the $Au_{329}(SR)_{84}$. Fragmentation in the MALDI process and low resolution at high mass range contribute to the broadness of peak. Nevertheless, the MALDI spectrum demonstrates the purity of the samples indicating the absence of lower or high mass impurities. ESI data shown in Figure 3 (right) confirms the MALDI spectrum. The envelope of peaks between 1:0.01 to 1:0.20 Au:Ag ratio nicely show the individual silver atom incorporation corresponding to the 89/4 m/z value. However as the silver atoms increases to 1:0.2, the baseline separation is lost and only part of the peaks are resolved. This type of loss of baseline separation has been observed before in the case of $Au_{144-x}Ag_x(SR)_{60}$.[31] In 1:0.33 and higher Au:Ag ratios, the peaks corresponding to Ag incorporation are not at all resolved, instead one broad peak is observed. However this broad peak moves to lower mass as expected in the 1:0.50 and 1:0.66 ratio. Only a poor signal is observed for the 1:0.66 ratio. No observable signal was present for the 1:1 ratio and upon extrapolation of the ESI data, we assumed a 1:1 Au:Ag distribution of atoms. We note that the Au:Ag ratio larger than 1:0.2 until 1:1, the resulting species are lower in stability compared to the lower Au:Ag ratios. Also, a large mass shift is observed between the 1:0.2 and 1:0.33 ratio. This pattern was also observed earlier[31] in $Au_{144-x}Ag_x(SR)_{60}$ and could be due to Ag atom induced structural differences, resulting in the dramatic changes in optical spectra, Figure 1. Further studies on the atomic structure and its dependence on composition is warranted.

Broad ESI peaks were observed in nanoparticles synthesis at higher Au:Ag incoming molar ratio (refer figure 3 and figure S1 for full spectrum from 13-27 kDa). The intrinsic broadening of the peaks as the number of silver atoms increase is due to the presence of isotopes, as observed before.[31] The center of the peak was used to calculate the average number of silver incorporation. This broadening might also be due to the several possible composition, but the broadening due to silver isotope is a stronger possibility. Nanomolecules synthesized at higher Au:Ag ratio are not stable upon prolong thermochemical treatment. Bond strength within nanomolecules falls under following order, Au-Au>Au-Ag>Ag-Ag.[26] Thus, the incorporation of larger number of Ag atoms leads to comparatively weak and unstable bonding compared to Au-Au interaction.

Figure S3 shows low magnification STEM images of $Au_{329-x}Ag_x(SC_2H_4C_6H_5)_{84}$ (Au:Ag 1:0.20, 1:0.50 and 1:1 ratio) showing the monodispersity of the synthesized samples. Average diameter of the nanoparticles was measured to be ~2 nm. The elemental composition of the nanomolecules synthesized using 1:0.20 and 1:0.66 ratio was determined by energy dispersive X-ray spectroscopy (EDS) coupled to the STEM. (See supporting information figure S4 and Table S1). STEM-EDS shows relative elemental composition of $Au_{\sim303}Ag_{\sim26}(SR)_{84}$ as Au (85%) and Ag (15 %). It shows 7 % deviation with respect to the ESI-MS measurement. Nanomolecules synthesis using Au:Ag ration of 1:0.66($Au_{\sim181}Ag_{\sim148}(SR)_{84}$ shows Au(67%) and Ag(33%). EDS process involved high energy electron shower to the selected areas of the TEM grid (i.e. nanoparticles) and emitted X-ray was counted as a function of photon energy which shows the relative Au and Ag composition. We notes that that alloy nanoparticle are unstable to the long STEM exposure time and eventually decomposed. This may be the reason for the deviation of the EDS and ESI-MS results. Also, ESI-MS assignments are based on most intense peak in determination of Au and Ag in elemental composition.

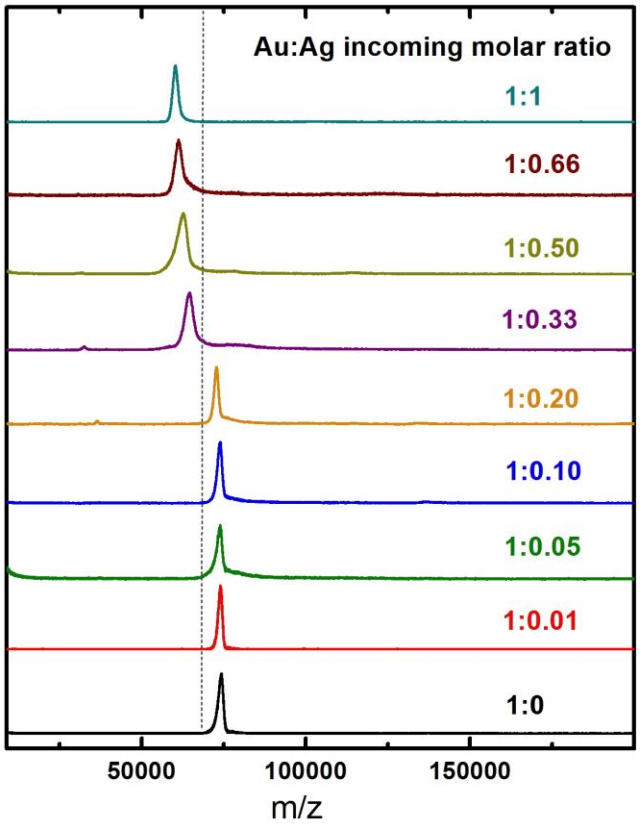

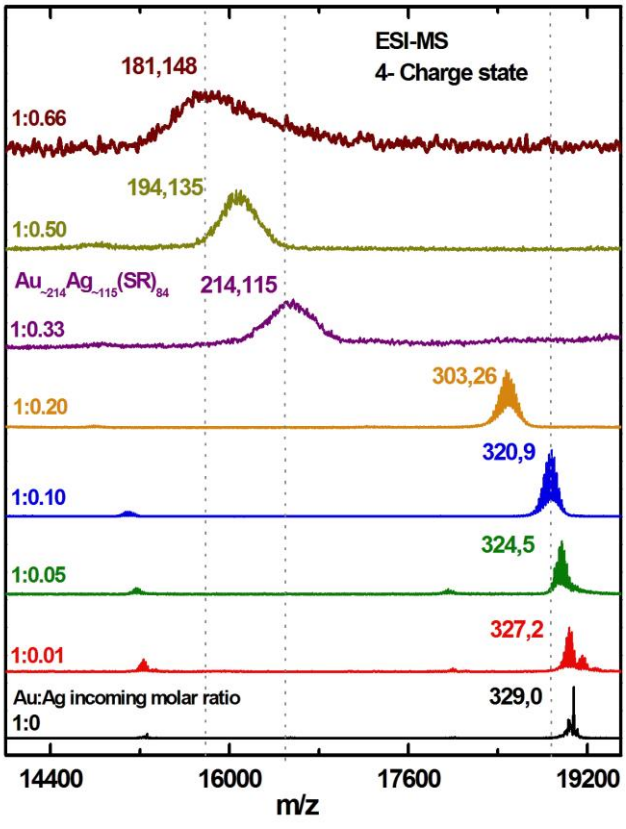

Figure 3. MALDI TOF (1+ ion on left) and Electrospray ionization (ESI) mass spectra (4- ions on right) of $Au_{329-x}Ag_x(SR)_{84}$ nanomolecules for Au:Ag precursor ratios of 1:0 (black), 1:0.01 (red), 1:0.05 (olive), 1:0.10 (blue) and 1:0.20 (orange),1:0.33 (purple) and 1:0.50 (dark yellow), 1 :0.66 (brown) and 1:1 (cyan) in the starting material. The number of Au and Ag atoms of most intense peak is denoted above each distribution of peaks.

In order to determine the morphology of $Au_{329-x}Ag_x(SR)_{84}$ molecules, we performed small-angle X-ray scattering (SAXS) measurements. Figure 4a show the SAXS profiles of the $Au_{329-x}Ag_x(SR)_{84}$ nanoparticles in comparison of $Au_{329}(SR)_{84}$. Nanoparticles synthesized using Au:Ag precursor ratios of 1:0.10, 1:0.66 and 1:1 are used as representative samples. The wide range of linear Guinier behavior (ln[I(q)] vs q^2, Fig. 4a inset and Fig. S5) and the scattering oscillation features at q of 0.4-0.9 $Å^{-1}$ (Fig. 4a) strongly suggest the high monodispersity of $Au_{329-x}Ag_x(SR)_{84}$ nanoparticles in solution ~~(refer figure S5)~~. The pair distance distribution function (PDDF) of these nanoparticles, an inverse Fourier transform of SAXS data, display a Gaussian-like profile, indicating $Au_{329-x}Ag_x(SR)_{84}$ nanoparticles adopt an ellipsoid-like shape, with the largest inner particle dimension about 3.0 ± 0.3 nm. ~~The PDDF of the various ratios, Figure 4b, all show uniform size, indicating the absence of impurities, such as larger plasmonic particles or other smaller 144 Au atom sizes.~~

The positions of peaks and valleys of SAXS profiles in q range of 0.4-0.9 $Å^{-1}$ shift toward higher q values with increasing number of silver atoms in particles, suggesting the particle sizes becomes slightly smaller. The radius of gyration, R_g, of the nanoparticle obtained from the SAXS Guinier fit, also reflect this subtle size change (Table S4): 9.5±0.2 Å for Au_{329} and 9.3±0.2 Å for Au:Ag=1:1. We reconstructed 3D bead models directly from the SAXS data using an *ab initio* program DAMMIN[39] for all these four nanomolecules and the bead models indeed all adopt ellipsoid-like shapes (Figure S7). A representative bead model of $Au_{329}(SR)_{84}$ is shown in Figure S6. However, the bead models do not have sufficient resolution to allow quantitative comparison on particle sizes. We employed ellipsoid models to fit the SAXS with the assumption of uniform electron density within the particles. SAXS modeling for individual nanomolecules are shown in Figure S8. Prolate ellipsoid models, in which one axis is longer than the other two equal length axes, best fit the data. The resulting ellipsoids have short axis diameter of 2.0-2.1 nm, and long axis length of 2.7-3.0 nm. The detailed parameters of ~~, and~~ these ~~resulting lengths of~~ ellipsoid models ~~axes and axis aspect ratios~~ are listed in Table S4. It is interesting to point out that, according to the fitting results, adding silver slightly elongates the particles while the particles become slimmer with higher silver content.

~~The important conclusion is that SAXS data shows that the size of all the particles are in the 2.2 ± 0.1 nm region, indicating the absence of larger or smaller nanoparticle impurities.~~

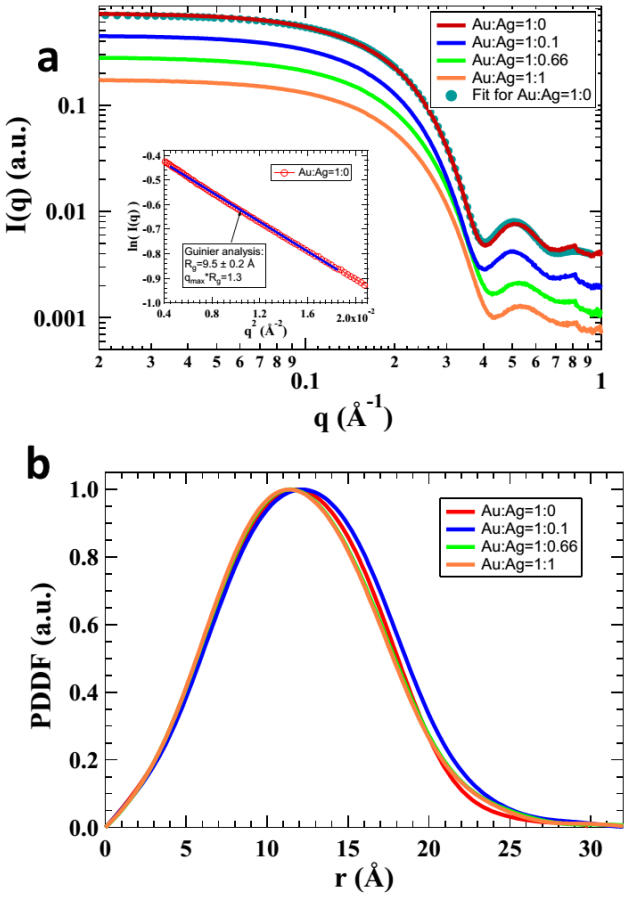

Figure 4. SAXS data, fittings and pair distance distribution functions of $Au_{329-x}Ag_x(SR)_{84}$ nanoparticles. (a) SAXS data of $Au_{329-x}Ag_x(SR)_{84}$ nanoparticles were collected up to 1.0 $Å^{-1}$. The curve of closed-circles in cyan color is the fitting for $Au_{329}(SR)_{84}$ using prolate ellipsoid model with uniform density, where axes a=b<c. The resulting ellipsoid is displayed in figure S6 in cyan mesh. The inset is the Guinier plot for $Au_{329}(SR)_{84}$ and the fit, i.e., $Ln[I(q)] = Ln[I(q=0)] - R_g^2q^2/3$ at q close to zero. (b) The pair distance distribution functions were derived from SAXS data in (A) using program GNOM.[40]

In conclusion we report unprecedented results of the high mass, plasmonic Au-Ag alloy composition with $Au_{329-x}Ag_x(SCH_2CH_2Ph)_{84}$. This is the first instance in which ESI-MS mass spectrometry was employed to determine composition of thiolated plasmonic alloy nanoparticles to the atomic level, with mass at 76 kDa. Approximately 50 % of silver could be incorporate to $Au_{329}(SR)_{84}$ plasmonic nanoparticles. Surface plasmonic resonance sharpens upon silver incorporation. The result demonstrates the next generation applications of mass

spectrometry toward the determination of nanoparticles composition to the atomic level. This plasmonic behavior of the title alloy nanocrystals with a molecular composition may open door for the interesting application in nano-optical devices, solar cells and catalysis.

EXPERIMENTAL SECTION

Chemicals: HPLC grade solvents such as methanol, acetone and toluene were obtained from Fisher Scientific. phenylethanemercaptan (Sigma Aldrich, ≥99%), Sodium borohydride ($NaBH_4$, Acros, 99%), and trans-2-[3[(4-tertbutylphenyl)-2-methyl-2-propenylidene]malononitrile (DCTB matrix) (Fluka≥99%) were purchased and used as received.

Synthesis: The synthesis of the $Au_{329-x}Ag_x(SR)_{84}$ involves three steps. The first step is the synthesis of crude product that contains polydisperse Au/Ag nanoparticles by modify version of the previously reported method. [16, 31] The second step is the thermochemical treatment of the crude product with excess thiol to remove meta-stable alloy clusters. Final step is solvent fractionation to isolate $Au_{329-x}Ag_x(SR)_{84}$ alloy nanomolecules.

Step 1. Aqueous solution (30 mL) containing $HAuCl_4$ and $AgNO_3$ (total metal concentration was set to 15 mM) was mixed with toluene solution (30 mL) of tetraoctylammonium bromide, TOABr (0.55 mmol). The initial molar ratios of Au:Ag precursors set to 1:0, 1:0.01, 1:0.05, 1:0.10, 1:0.20,1:0.33,1:0.50, 1:0.66 and 1:1. After stirring for 30 min, the turbid organic phase was separated and phenylethane thiol (0.45 mmol) was added and further stirred for 30 min at room temperature (total metal to thiol molar ratio was set to 1:1). This solution was cooled in ice bath for 30 min. An aqueous solution of $NaBH_4$ (10 mmol, 20 mL) cooled to 0^oC, was rapidly added to the reaction mixture under vigorous stirring. After 3 hours, the organic layer was separated and evaporated to dryness. The product was washed with methanol to remove other byproducts. Then product was extracted with toluene.
Step 2: Typically,~*200* mg of crude products was dissolved in 0.50 mL of toluene and subjected to thermochemical treatment[41] with excess phenylethane thiol (0.50 mL) at 60-80^oC under stirring, while monitoring with MALDI-MS (figure S9). After meta-stable clusters disappeared (~3 hour to 8 days that depend on Au:Ag molar ratio), thermochemical treatment was discontinued and washed with methanol several times (2-4 times).
Step 3: Then product was dissolved in toluene and subjected to solvent fractionation with MeOH to isolate pure $Au_{329-x}Ag_x(SR)_{84}$ nanoalloy.

Following modification were made to the synthesis and isolation protocol to yield $Au_{329-x}Ag_x(SR)_{84}$.
(1) *Sequentially addition of Ag in the initial stage of synthesis*: The initial molar ratios of Au:Ag precursors set to 1:0, 1:0.01, 1:0.05, 1:0.10, 1:0.20,1:0.33,1:0.50, 1:0.66 and 1:1 . The reason for selecting such a broad ratio is to gain the "*insight* into silver incorporation" via mass spectrometry and Uv-visible spectrometry. These ratio can be further subdivide into three group based on mass spectrometry and Uv-visible spectrometric results. (a) 1:0, 1:0.01, 1:0.05, 1:0.10, 1:0.20 (b) 1:0.33 and 1:0.50, (c) 1:0.66 and 1:1.
(2) *Dynamic etching protocol depend on Au:Ag incoming molar ratio*: Etching protocol were modified to improve the $Au_{329-x}Ag_x(SR)_{84}$ yield at high Au:Ag ratio as follow. (a) Ratio 1:0, 1:0.01, 1:0.05, 1:0.10 and1:0.20: Nanomolecules subjected to thermochemical treatment up to eight days as usual. (b) Ratio 1:0.33 and 1:0.50: subjected to thermochemical treatment for two days while monitoring the MALDI-MS. If required re-etch for another 2-3 days to get clear baseline separation between different nanoparticles. (c) Ratio 1:0.66 and 1:1: thermochemical treatments were limited to 3-9 hours. Further thermochemical treatment lead to the decomposition.
(3) Systematic separation of the AuAg alloy to yield $Au_{329-x}Ag_x(SR)_{84}$:There were 3-4 types of alloy nanomolecules left after the thermochemical treatment at 11, 30-35, 60-73 and ~ 105 kDa mass ranges. However, relative types and amounts varied depend on the incoming Au:Ag ratio (Refer figure S9 for product related to the Au:Ag, 1:0.66 ratio). Thus, other nanoparticles were systematically removed or precipitated out from the mixture to obtained $Au_{329-x}Ag_x(SR)_{84}$ in pure form. At least 10-15 solvent fractionations cycles were performed for the $Au_{329-x}Ag_x(SR)_{84}$ isolation. The first set of solvent fractionation focus on systematic removal of 11 and 30-36 kDa alloy from the polydispersed mixture by dissolving the product in toluene and precipitating by MeOH. After then, possible larger nanoparticles (>76.3 kDa) were precipitated using the same solvent mixtures and pure $Au_{329-x}Ag_x(SR)_{84}$ were isolated.

Characterization
Mass spectrometric analysis: MALDI mass spectra were acquired with a Bruker Daltonics Autoflex mass spectrometer using DCTB matrix at optimal laser fluence. Spectral analyses were done using Bruker Daltonics flexAnalysis version 3.0. *At least 500 individual spectra were collected and averaged for analysis.*

ESI mass spectra were obtained from a Waters Synapt mass spectrometer in 50:50 toluene: CH_3CN solution in negative mode. ESI calibration was performed with 50:50 isopropanol:water solution of NaI. Calibration check was performed with $Au_{25}(SCH_2CH_2Ph)_{18}$ and $Au_{144}(SCH_2CH_2Ph)_{60}$. MS chromatogram were recorded over 5 min time period and averaged to acquired quality data with good signal to noice ratio.

Optical spectroscopy: UV-visible spectra were obtained in toluene solutions using Shimadzu UV-1601 spectrophotometer and UV probe 2.0 software in the 300–1100 nm range.

Scanning transmission electron microscopy analysis: Sample suitable for STEM analysis were prepared by drop casting a toluene solution of nanoparticles suspension onto lacey carbon films supported on 3 mm Cu grids. HAADF-STEM images and EDS spectra were acquired in a JEOL JEM-2200FS with a CEOS aberration corrector on the probe-forming system and Bruker XFlash SDD detector. Images were analyzed using ImageJ software (version 1.46r). EDS spectra were used to verify the presence of silver, using standardless routines in the Bruker Esprit software.

Small angle X-ray scattering: The SAXS measurements were performed at the 12ID-B beam line of Advanced Photon Source (APS) at Argonne National Laboratory, using 14 keV X-ray energy. The SAXS data were collected with Pilatus 2M detector (DECTRIS Ltd.) cut-off energy was set as 10 keV to eliminate possible fluorescence background. The beam size with 0.05 x 0.2 mm^2 and exposure times of 1s used for the measurement. The data were fully corrected, reduced to intensity vs scattering vector (q) profiles, and background subtracted, using the software package at the beamline.

Significant efforts made in the past four years to grow X-ray quality single crystals have been unsuccessful. The availability of X-ray structure will facilitate the theoretical analysis of the optical behavior. Thermogravimetric analysis and XPS measurements were not conducted due to the limited amount of the sample, however qualitative EDS studies were conducted to confirm the presence of silver, in addition to ESI-MS and MALDI-MS data.

ASSOCIATED CONTENT
Supporting Information
This material is available free of charge via the Internet at http://pubs.acs.org

AUTHOR INFORMATION
Corresponding Author
*E-mail: amal@olemiss.edu.
Notes
The authors declare no competing financial interest

ACKNOWLEDGEMENTS
C.K. and A.D. gratefully acknowledge support from NSF CHE-1255519. Electron microscopy research supported through a user project supported by ORNL's Center for Nanophase Materials Sciences (CNMS), which is sponsored by the Scientific User Facilities Division, Office of Basic Energy Sciences, U.S. Department of Energy. Work performed at Argonne and the use of the Advanced Photon Source, an Office of Science User Facility operated for the U.S. Department of Energy (DOE) Office of Science by Argonne National Laboratory, was supported by the U.S. DOE under Contract No. DE-AC02-06CH11357.

REFERENCES

(1) Jain, P. K.; Huang, X.; El-Sayed, I. H.; El-Sayed, M. A. Noble Metals on the Nanoscale: Optical and Photothermal Properties and Some Applications in Imaging, Sensing, Biology, and Medicine. *Acc. Chem. Res.* 2008, 41, 1578-1586.
(2) Hutter, E.; Fendler, J. H. Exploitation of Localized Surface Plasmon Resonance. *Adv. Mater.* 2004, 16, 1685-1706.
(3) Whetten, R. L.; Khoury, J. T.; Alvarez, M. M.; Murthy, S.; Vezmar, I.; Wang, Z. L.; Stephens, P. W.; Cleveland, C. L.; Luedtke, W. D.; Landman, U. Nanocrystal gold molecules. *Adv. Mater.* 1996, 8, 428-433.
(4) Alvarez, M. M.; Khoury, J. T.; Schaaff, T. G.; Shafigullin, M. N.; Vezmar, I.; Whetten, R. L. Optical absorption spectra of nanocrystal gold molecules. *J. Phys. Chem. B* 1997, 101, 3706-3712.
(5) Weissker, H. C.; Escobar, H. B.; Thanthirige, V. D.; Kwak, K.; Lee, D.; Ramakrishna, G.; Whetten, R. L.; López-Lozano, X. Information on quantum states pervades the visible spectrum of the ubiquitous $Au_{144}(SR)_{60}$ gold nanocluster. *Nat Commun* 2014, 5.
(6) Murray, R. W. Nanoelectrochemistry: Metal nanoparticles, nanoelectrodes, and nanopores. *Chem. Rev.* 2008, 108, 2688-2720.

(7) Knoppe, S.; Bürgi, T. Chirality in Thiolate-Protected Gold Clusters. *Acc. Chem. Res.* 2014, 47, 1318-1326.

(8) Yamazoe, S.; Koyasu, K.; Tsukuda, T. Nonscalable Oxidation Catalysis of Gold Clusters. *Acc. Chem. Res.* 2013, 47, 816-824.

(9) Li, G.; Jin, R. Atomically Precise Gold Nanoclusters as New Model Catalysts. *Acc. Chem. Res.* 2013, 46, 1749-1758.

(10) Negishi, Y.; Kurashige, W.; Niihori, Y.; Nobusada, K. Toward the creation of stable, functionalized metal clusters. *Phys. Chem. Chem. Phys.* 2013, 15, 18736-18751.

(11) Negishi, Y.; Iwai, T.; Ide, M. Continuous modulation of electronic structure of stable thiolate-protected Au_{25} cluster by Ag doping. *Chem. Commun.* 2010, 46, 4713-4715.

(12) Kumara, C.; Aikens, C. M.; Dass, A. X-ray Crystal Structure and Theoretical Analysis of $Au_{25-x}Ag_x(SCH_2CH_2Ph)_{18}^-$ Alloy. *J. Phys. Chem. Lett.* 2014, 5, 461-466.

(13) Negishi, Y.; Munakata, K.; Ohgake, W.; Nobusada, K. Effect of Copper Doping on Electronic Structure, Geometric Structure, and Stability of Thiolate-Protected Au25 Nanoclusters. *J. Phys. Chem. Lett.* 2012, 3, 2209-2214.

(14) Negishi, Y.; Kurashige, W.; Niihori, Y.; Iwasa, T.; Nobusada, K. Isolation, structure, and stability of a dodecanethiolate-protected Pd_1Au_{24} cluster. *Phys. Chem. Chem. Phys.* 2010, 12, 6219-6225.

(15) Qian, H.; Jiang, D.-e.; Li, G.; Gayathri, C.; Das, A.; Gil, R. R.; Jin, R. Monoplatinum Doping of Gold Nanoclusters and Catalytic Application. *J. Am. Chem. Soc.* 2012, 134, 16159-16162.

(16) Dass, A. Faradaurate Nanomolecules: A Superstable Plasmonic 76.3 kDa Cluster. *J. Am. Chem. Soc.* 2011, 133, 19259-19261.

(17) Kumara, C.; Dass, A. $Au_{329}(SR)_{84}$ Nanomolecules: Compositional Assignment of the 76.3 kDa Plasmonic Faradaurates. *Anal. Chem.* 2014, 86, 4227-4232.

(18) Kumara, C.; Zuo, X.; Ilavsky, J.; Chapman, K. W.; Cullen, D. A.; Dass, A. Super-Stable, Highly Monodisperse Plasmonic Faradaurate-500 Nanocrystals with 500 Gold Atoms: $Au_{\sim 500}(SR)_{\sim 120}$. *J. Am. Chem. Soc.* 2014, 136, 7410-7417.

(19) Kumara, C.; Zuo, X.; Cullen, D. A.; Dass, A. Faradaurate-940: Synthesis, Mass Spectrometry, Electron Microscopy, High-Energy X-ray Diffraction, and X-ray Scattering Study of $Au_{\sim 940\pm 20}(SR)_{\sim 160\pm 4}$ Nanocrystals. *ACS Nano* 2014, 8, 6431-6439.

(20) Walter, M.; Akola, J.; Lopez-Acevedo, O.; Jadzinsky, P. D.; Calero, G.; Ackerson, C. J.; Whetten, R. L.; Gronbeck, H.; Hakkinen, H. A unified view of ligand-protected gold clusters as superatom complexes. *Proc. Natl. Acad. Sci. U.S.A.* 2008, 105, 9157-9162.

(21) Jadzinsky, P. D.; Calero, G.; Ackerson, C. J.; Bushnell, D. A.; Kornberg, R. D. Structure of a thiol monolayer-protected gold nanoparticle at 1.1 angstrom resolution. *Science* 2007, 318, 430-433.

(22) Heaven, M. W.; Dass, A.; White, P. S.; Holt, K. M.; Murray, R. W. Crystal structure of the gold nanoparticle $[N(C_8H_{17})_4][Au_{25}(SCH_2CH_2Ph)_{18}]$. *J. Am. Chem. Soc.* 2008, 130, 3754-3755.

(23) Qian, H.; Zhu, M.; Wu, Z.; Jin, R. Quantum Sized Gold Nanoclusters with Atomic Precision. *Acc. Chem. Res.* 2012, 45, 1470-79.

(24) Jin, R. Quantum sized, thiolate-protected gold nanoclusters. *Nanoscale* 2010, 2, 343-362.

(25) Malola, S.; Lehtovaara, L.; Enkovaara, J.; Häkkinen, H. Birth of the Localized Surface Plasmon Resonance in Monolayer-Protected Gold Nanoclusters. *ACS Nano* 2013, 7, 10263-10270.

(26) Ferrando, R.; Jellinek, J.; Johnston, R. L. Nanoalloys: From Theory to Applications of Alloy Clusters and Nanoparticles. *Chem. Rev.* 2008, 108, 845-910.

(27) Tracy, J. B.; Kalyuzhny, G.; Crowe, M. C.; Balasubramanian, R.; Choi, J. P.; Murray, R. W. Poly(ethylene glycol) ligands for high-resolution nanoparticle mass spectrometry. *J. Am. Chem. Soc.* 2007, 129, 6706-6707.

(28) Dass, A.; Stevenson, A.; Dubay, G. R.; Tracy, J. B.; Murray, R. W. Nanoparticle MALDI-TOF mass spectrometry without fragmentation: $Au_{25}(SCH_2CH_2Ph)_{18}$ and mixed monolayer $Au_{25}(SCH_2CH_2Ph)_{18-x}(L)_x$. *J. Am. Chem. Soc.* 2008, 130, 5940-5946.

(29) Chaki, N. K.; Negishi, Y.; Tsunoyama, H.; Shichibu, Y.; Tsukuda, T. Ubiquitous 8 and 29 kDa gold: Alkanethiolate cluster compounds: Mass-spectrometric determination of molecular formulas and structural implications. *J. Am. Chem. Soc.* 2008, 130, 8608-8610.

(30) Kumara, C.; Dass, A. AuAg alloy nanomolecules with 38 metal atoms. *Nanoscale* 2012, 4, 4084-4086.

(31) Kumara, C.; Dass, A. $(AuAg)_{144}(SR)_{60}$ alloy nanomolecules. *Nanoscale* 2011, 3064-3067.

(32) Knoppe, S.; Boudon, J.; Dolamic, I.; Dass, A.; Bürgi, T. Size Exclusion Chromatography for Semipreparative Scale Separation of $Au_{38}(SR)_{24}$ and $Au_{40}(SR)_{24}$ and Larger Clusters. *Anal. Chem.* 2011, 83, 5056-5061.

(33) Durante, N.; Fortunelli, A.; Broyer, M.; Stener, M. Optical Properties of Au Nanoclusters from TD-DFT Calculations. *J. Phys. Chem. C.* 2011, 115, 6277-6282.

(34) Aikens, C. M.; Li, S.; Schatz, G. C. From Discrete Electronic States to Plasmons: TDDFT Optical Absorption Properties of Ag n (n = 10, 20, 35, 56, 84, 120) Tetrahedral Clusters. *J. Phys. Chem. C.* 2008, 112, 11272-11279.

(35) Cortie, M. B.; McDonagh, A. M. Synthesis and Optical Properties of Hybrid and Alloy Plasmonic Nanoparticles. *Chem. Rev.* 2011, 111, 3713-3735.

36. Shore, M. S.; Wang, J.; Johnston-Peck, A. C.; Oldenburg, A. L.; Tracy, J. B. Synthesis of Au(Core)/Ag(Shell) Nanoparticles and their Conversion to AuAg Alloy Nanoparticles. *Small* 2011, 7, 230-234.

(37) Malola, S.; Häkkinen, H. Electronic Structure and Bonding of Icosahedral Core–Shell Gold–Silver Nanoalloy Clusters Au144–xAgx(SR)60. *J. Phys. Chem. Lett.* 2011, 2, 2316-2321.

(38) Link, S.; Wang, Z. L.; El-Sayed, M. A. Alloy Formation of Gold−Silver Nanoparticles and the Dependence of the Plasmon Absorption on Their Composition. *J. Phys. Chem. B.* 1999, 103, 3529-3533.

(39) Svergun, D. I. Restoring Low Resolution Structure of Biological Macromolecules from Solution Scattering Using Simulated Annealing. *Biophys. J.* 76, 2879-2886.

(40) Svergun, D. Determination of the regularization parameter in indirect-transform methods using perceptual criteria. *J. Appl. Crystallogr.* 1992, 25, 495-503.

(41) Schaaff, T. G.; Whetten, R. L. Controlled etching of Au : SR cluster compounds. *J. Phys. Chem. B* 1999, 103, 9394-9396.